

Detecting British Columbia Coastal Rainfall Patterns by Clustering Gaussian Processes

Forrest Paton and Paul D. McNicholas

Department of Mathematics and Statistics, McMaster University, Hamilton, Ontario, Canada.

Abstract

Functional data analysis is a statistical framework where data are assumed to follow some functional form. This method of analysis is commonly applied to time series data, where time, measured continuously or in discrete intervals, serves as the location for a function's value. Gaussian processes are a generalization of the multivariate normal distribution to function space and, in this paper, they are used to shed light on coastal rainfall patterns in British Columbia (BC). Specifically, this work addressed the question over how one should carry out an exploratory cluster analysis for the BC, or any similar, coastal rainfall data. An approach is developed for clustering multiple processes observed on a comparable interval, based on how similar their underlying covariance kernel is. This approach provides significant insights into the BC data, and these insights can be described in terms of El Niño and La Niña; however, the result is not simply one cluster representing El Niño years and another for La Niña years. From one perspective, the results show that clustering annual rainfall can potentially be used to identify extreme weather patterns.

Keywords: British Columbia; Clustering; Coastal Rainfall; El Niño; Extreme weather; Gaussian processes; La Niña; Mixture model.

1 Introduction

The term El Niño (literally “The Boy” in Spanish) was first recognized on the Pacific coastal region of South America. The term El Niño refers more specifically to the “Christ child” because this phenomenon, of irregularly warm south Pacific Ocean temperatures, tends to start near Christmas. In contrast to predictable yearly seasonal changes, El Niño does not occur at regular intervals. This is particularly problematic for policy makers, businesses, and people who rely on calculable, foreseeable weather patterns. For example, seasonal changes can specifically alter food production plans, such as when to deploy fishing vessels or harvest crops. While El Niño is primarily categorized through warming temperatures in the eastern

and equatorial Pacific Ocean, its effects can be seen around the globe through teleconnections. Teleconnections are an environmental phenomena that describe correlated large-scale atmospheric changes over non-contiguous geographic regions. While some teleconnections are well established, others rely on observing statistical irregularities (Gudmundson and Babkina, 2003; Ward et al., 2014); namely, El Niño’s affect on precipitation patterns. Sir Gilbert Walker, a 20th century English scientist, for example, first identified the link between Asian monsoons and Pacific coastal barometer readings (Gudmundson and Babkina, 2003). However, the study of teleconnections, such as precipitation patterns, is notoriously complex because of intricate spatial and temporal correlations. Understanding El Niño’s effect on distant precipitation can shed light on these patterns. Specifically, classifying irregular precipitation patterns in the Americas can help understand El Niño’s impact on local weather systems.

A question of particular interest is: which years exhibit distinct rainfall patterns? For prediction, knowing how Pacific Ocean changes affect rainfall can have significant implications. A model for clustering yearly rainfall data will also give insight to research on the mechanistic properties of teleconnections. This problem has overlap in the statistical field of functional data clustering, where data are assumed to follow some functional form. Herein, mixture model-based clustering provides an effective approach to cluster data, and Gaussian Processes provide a model for rainfall. Specifically, the use of Gaussian processes (GPs) gives a probabilistic starting point. A GP is a stochastic process that generalizes a finite-dimensional normal distribution to function space. GPs have been used to successfully solve complex non-linear regression and classification problems (Rasmussen, 2005). When multiple functions exist on the same interval, usually compact $[0, T]$ and finite, it can be useful to classify them into a finite number of mutually exclusive groups. Here the process would be defined on the index set time, specifically the months of the year.

2 Background

2.1 Gaussian Process

Rasmussen (2005) defines a GP as: “... a collection of random variables, any finite number of which have a joint Gaussian distribution”. A GP $\mathbf{f}(\mathbf{x})$ creates a set of random variables evaluated at \mathbf{x} . In essence, a GP is a distribution over functions, i.e.,

$$\mathbf{f}(\mathbf{x}) \sim \mathcal{GP}(m(\mathbf{x}), k(\mathbf{x}, \mathbf{x}')). \quad (1)$$

A GP is defined by its mean function and covariance kernel:

$$m(\mathbf{x}) = \mathbb{E}[f(\mathbf{x})], \quad (2)$$

$$k(\mathbf{x}, \mathbf{x}') = \mathbb{E}[(f(\mathbf{x}) - m(\mathbf{x}))(f(\mathbf{x}') - m(\mathbf{x}'))]. \quad (3)$$

A common GP, and the kernel considered in this paper, is defined with mean function $\mathbf{0}$ and squared exponential (SE) covariance function:

$$k(\mathbf{x}_i, \mathbf{x}_j) = \sigma_f^2 \exp\left(-\frac{1}{2l^2}|\mathbf{x}_i - \mathbf{x}_j|^2\right) + \sigma_n^2 \delta_{ij}. \quad (4)$$

The SE kernel is a widely used (Rasmussen, 2005). One convenient property of the SE kernel is infinite differentiability, which is useful because the first derivative is needed for hyper-parameter estimation. Here, the use of the term hyper-parameter refers to a set of parameters that make up the “non-parametric model”. That is, the hyper-parameters only appear in the model’s prior and, as shown later in (7), are integrated out of the final model (posterior). The covariance kernel, for example, is defined by the following set of hyper-parameters which control the shape of the process: σ_f^2 is the height parameter, l is the length-scale parameter, σ_n^2 is the measurement noise, and

$$\delta_{ij} = \begin{cases} 1 & \text{if } i = j, \\ 0 & \text{otherwise} \end{cases}.$$

Although the SE is the most popular, different kernel functions can be used. Because the kernel is needed to populate a multivariate normal distribution covariance matrix, the kernel is restricted to produce positive semi-definite matrices. While the SE covariance kernel is a popular choice, modelling the shape of the covariance kernel is an open ended problem. One systematic solution can be formed by considering a Bayesian model selection framework as discussed in Rasmussen (2005). For the SE covariance kernel, σ_f^2 controls the height or the amplitude of the GP, l controls the length-scale, and the hyper-parameter σ_n^2 adds measurement noise to the function output y . Here, y is the value of the function f with additive noise: $y = f + \sigma_n^2$. If the observed value y is perfectly interpolated from the GP, i.e., if $y = f$, then $\sigma_n^2 = 0$. This kernel is used to construct a matrix, \mathbf{K} , which will serve as the variance covariance matrix in a multivariate normal distribution introduced in the next section:

$$\mathbf{K} = \begin{pmatrix} k(x_1, x_1) & \cdots & k(x_1, x_n) \\ \vdots & \ddots & \vdots \\ k(x_n, x_1) & \cdots & k(x_n, x_n) \end{pmatrix}.$$

While a GP is defined on the entire real line, we only observe a finite amount n of realizations $\mathbf{x} = (x_1, \dots, x_n)'$, and corresponding $\mathbf{y} = (y_1, \dots, y_n)'$. The vector \mathbf{x} is commonly called the input and represents the location of the the process, i.e., observation $y_i = f(x_i)$. The vector \mathbf{y} is referred to as the output, and is the function evaluated at location \mathbf{x} . This allows for a generalization to a multivariate normal distribution via $f(\mathbf{x}) \sim \mathcal{MVN}(\mathbf{0}, \mathbf{K})$. This is possible because marginalizing a Gaussian distribution is trivial: the resulting distribution is Gaussian and we can ignore the (x, y) pairs that are unobserved or missing. Here

changing the kernel effects the shape of the function, effectively controlling the magnitude of which observations x_i and x_j are correlated. Formulating the problem in this way, we can see the kernel is our prior on the function space, and the (marginal) likelihood for the GP comes after conditioning on the realized points. As shown in the next section, the hyper-parameters are often estimated to maximize the likelihood of the GP.

2.2 Likelihood

The previous section introduced the kernel function and how it relates to a prior on function space and how the hyper-parameters effect the correlation between the input \mathbf{x} and outcome \mathbf{y} . Now, the likelihood for a GP will be introduced and strategies for choosing the hyper-parameters will be illustrated. From the definition of a GP, $\mathbf{y} \sim \mathcal{N}(\mathbf{0}, \mathbf{K})$, which will be shown formally below. First, let $\mathbf{f} \sim \mathcal{N}(\mathbf{0}, \mathbf{K}_*)$, where \mathbf{K}_* is the covariance matrix constructed from the noiseless SE kernel:

$$k(x_i, x_j) = \sigma_f^2 \exp\left(-\frac{1}{2l^2}|x_i - x_j|^2\right)$$

such that $\mathbf{K} \triangleq \mathbf{K}_* + \mathbf{I}\sigma_n^2$.

The likelihood for a GP is conditioned on the observed values to obtain a marginal likelihood, using ϕ to denote the normal density function:

$$p(\mathbf{f} | \mathbf{x}) = \underbrace{\phi(\mathbf{f} | \mathbf{0}, \mathbf{K}_*)}_{\text{function prior}}, \quad (5)$$

$$p(\mathbf{y} | \mathbf{f}) = \underbrace{\prod_{i=1}^n \phi(y_i | f_i, \sigma_n^2)}_{\text{likelihood}}. \quad (6)$$

We get the marginal for \mathbf{y} by using Bayes' rule and integrating over \mathbf{f} :

$$p(\mathbf{y} | \mathbf{x}) = \int p(\mathbf{y} | \mathbf{f}, \mathbf{x}) p(\mathbf{f} | \mathbf{x}) d\mathbf{f}. \quad (7)$$

Taking the log of (7) gives

$$\log p(\mathbf{y}_i | \mathbf{x}) = -\frac{1}{2} \left\{ \mathbf{y}_i \mathbf{K}^{-1} \mathbf{y}_i^\top + \log |\mathbf{K}| + n \log 2\pi \right\}. \quad (8)$$

This likelihood can be broken down into three main components, the data fit term, model complexity term, and a constant term:

$$\log p(\mathbf{y}_i | \mathbf{x}) = -\frac{1}{2} \left\{ \underbrace{\mathbf{y}_i \mathbf{K}^{-1} \mathbf{y}_i^\top}_{\text{data fit}} + \underbrace{\log |\mathbf{K}|}_{\text{complexity}} + \underbrace{n \log 2\pi}_{\text{constant}} \right\}. \quad (9)$$

The data fit and complexity component share an interesting tradeoff. For small length-scale values l , the model will fit the data well and the data fit component will be small. However, points will not be considered “near” each other, resulting in a high model complexity. Conversely, if l is large (suggesting no correlation between points), then the complexity will be small but the data fit term will be large. This is because the SE kernel $k(\mathbf{x}_i, \mathbf{x}_j)$ will converge to σ_f^2 , turning \mathbf{K} into a diagonal matrix. Because GPs have these inherent penalty terms for over- and under-fitting, cross validation methods are generally not needed.

2.3 Predictive Distribution

GPs are commonly used in supervised regression tasks for their ability to non-parametrically approximate complex functions and solve functional engineering problems (Bin and Wenlai, 2013). It is often of interest to infer the function’s value outside of the paired training data (\mathbf{x}, \mathbf{y}) . To do this, a predictive distribution can be constructed. Let $\mathbf{y}_* = \mathbf{f}(\mathbf{x}_*)$ be the unobserved outputs to be inferred at locations \mathbf{x}_* . The distribution can easily be derived through probabilistic terms. From properties of joint Gaussians

$$\mathbf{f}(\mathbf{x}) \sim \mathcal{N}(\mathbf{0}, \mathbf{K}(\mathbf{x}, \mathbf{x})), \quad (10)$$

$$\mathbf{f}(\mathbf{x}_*) \sim \mathcal{N}(\mathbf{0}, \mathbf{K}(\mathbf{x}_*, \mathbf{x}_*)), \quad (11)$$

$$\begin{bmatrix} \mathbf{f}(\mathbf{x}) \\ \mathbf{f}(\mathbf{x}_*) \end{bmatrix} \sim \mathcal{N}\left(\mathbf{0}, \begin{bmatrix} \mathbf{K}(\mathbf{x}, \mathbf{x}) & \mathbf{K}(\mathbf{x}, \mathbf{x}_*) \\ \mathbf{K}(\mathbf{x}_*, \mathbf{x}) & \mathbf{K}(\mathbf{x}_*, \mathbf{x}_*) \end{bmatrix}\right). \quad (12)$$

Note that (12) is the joint distribution of the observed pairs (\mathbf{x}, \mathbf{y}) and unobserved $\mathbf{f}(\mathbf{x}_*)$ at location \mathbf{x}_* . The expected value for $\mathbf{f}(\mathbf{x}_*)$ can be derived using conditional properties which leads to

$$\hat{\mathbf{f}}(\mathbf{x}_*) \triangleq \mathbb{E}[\mathbf{f}(\mathbf{x}_*) | \mathbf{x}, \mathbf{y}, \mathbf{x}_*] = \mathbf{K}(\mathbf{x}_*, \mathbf{x})[\mathbf{K}(\mathbf{x}, \mathbf{x})]^{-1}\mathbf{y}; \quad (13)$$

a complete derivation is given by Rasmussen (2005). Then, (13) can then be used to compute estimates for the function’s value $\mathbf{f}(\mathbf{x}_*)$ at location \mathbf{x}_* .

2.4 Model-Based Clustering

Clustering is an unsupervised machine learning task which attempts to classify unlabelled data points into distinct groups. Commonly, clustering is defined as assigning data into groups such that data in the same cluster are more similar to each other than to data in a different cluster. Initially this definition seems intuitive; however, practically there are some problems. Namely, grouping each data point into its own cluster would satisfy this definition. Instead, McNicholas (2016a) provides a definition not based on similarity:

A cluster is a unimodal component within an appropriate finite mixture model.

The use of the word appropriate here requires consideration of the data:

It means that the model has the necessary flexibility, or parameterization, to fit the data

(McNicholas, 2016a). In either case, many methods have been developed to tackle this problem of unsupervised learning. Model-based refers to using probability distributions to model the clusters (as opposed to hierarchical, k -means, etc.).

2.5 Finite Mixture Model

The finite mixture model is a popular tool for (model-based) clustering (see McNicholas, 2016b). The density of a G -component finite mixture model is

$$f(\mathbf{x}|\boldsymbol{\varphi}) = \sum_{g=1}^G \pi_g f_g(\mathbf{x}|\boldsymbol{\theta}_g), \quad (14)$$

where $\pi_g > 0$ is the g th mixing proportion, with $\sum_{g=1}^G \pi_g = 1$, $f_g(\mathbf{x}|\boldsymbol{\theta}_g)$ is the g th component density, and $\boldsymbol{\theta} = (\boldsymbol{\theta}_1, \dots, \boldsymbol{\theta}_G)$ are the component density-specific parameters, with $\boldsymbol{\varphi} = (\boldsymbol{\pi}, \boldsymbol{\theta})$ and $\boldsymbol{\pi} = (\pi_1, \dots, \pi_G)$. The likelihood is given by

$$\mathcal{L}(\boldsymbol{\varphi}) = \prod_{i=1}^n \sum_{g=1}^G \pi_g \phi(\mathbf{x}_i \mid \boldsymbol{\mu}_g, \boldsymbol{\Sigma}_g). \quad (15)$$

2.6 Expectation-Maximization

Model-based clustering requires estimating the unknown model parameters from the mixture density in (14). The expectation-maximization (EM) algorithm (Dempster et al., 1977) provides a good starting point for this problem. The two-step algorithm first starts by computing the expectation of the complete-data log-likelihood (E-step), then maximizes the expectation of the complete-data log-likelihood (M-step). The E- and M-steps are iterated until some stopping rule is met. Consider a Gaussian model-based clustering complete-data likelihood, denoted by \mathcal{L}_c , where the complete-data comprise the observed $\mathbf{x}_1, \dots, \mathbf{x}_n$ together with the missing labels $\mathbf{z}_1, \dots, \mathbf{z}_n$, where $\mathbf{z}_i = (z_{i1}, \dots, z_{iG})$ and $z_{ig} = 1$ if observation i belongs to component g and $z_{ig} = 0$ otherwise. Now,

$$\mathcal{L}_c(\boldsymbol{\varphi}) = \prod_{i=1}^n \sum_{g=1}^G [\pi_g \phi(\mathbf{x}_i \mid \boldsymbol{\mu}_g, \boldsymbol{\Sigma}_g)]^{z_{ig}}. \quad (16)$$

Of course, if $\mathbf{z}_1, \dots, \mathbf{z}_n$ were known, then \mathcal{L}_c could easily be maximized by splitting the data into their respective groups and MLE estimates or some continuous optimizer could be used.

However, because $\mathbf{z}_1, \dots, \mathbf{z}_n$ is unknown the EM algorithm is often used. In the E-step, we compute

$$\hat{z}_{ig} := \mathbb{E}[Z_{ig} | \mathbf{x}_i] = \frac{\hat{\pi}_g \phi(\mathbf{x}_i | \hat{\boldsymbol{\mu}}_g, \hat{\boldsymbol{\Sigma}}_g)}{\sum_{h=1}^G \hat{\pi}_h \phi(\mathbf{x}_i | \hat{\boldsymbol{\mu}}_h, \hat{\boldsymbol{\Sigma}}_h)}. \quad (17)$$

Next, in the “maximization” step, the parameters are updated. This amounts to estimating the covariance matrix and mean vector for a Gaussian mixture model. In the M-step, the updates are:

$$\hat{\pi}_g = \frac{n_g}{n}, \quad (18)$$

$$\hat{\boldsymbol{\mu}}_g = \frac{1}{n_g} \sum_{i=1}^n \hat{z}_{ig} \mathbf{x}_i, \quad (19)$$

$$\hat{\boldsymbol{\Sigma}}_g = \frac{1}{n_g} \sum_{i=1}^n \hat{z}_{ig} (\mathbf{x}_i - \hat{\boldsymbol{\mu}}_g)(\mathbf{x}_i - \hat{\boldsymbol{\mu}}_g)^\top, \quad (20)$$

where $n_g = \sum_{i=1}^n \hat{z}_{ig}$. After parameter estimation is completed, the clustering results are expressed through the probabilities \hat{z}_{ig} , i.e., \hat{z}_{ig} is the probability that \mathbf{x}_i belongs to component g . These soft probabilities ($\hat{z}_{ig} \in [0, 1]$) are often converted into hard classifications via maximum *a posteriori* probabilities:

$$\text{MAP}(\hat{z}_{ig}) = \begin{cases} 1 & \text{if } g = \text{argmax}_h(\hat{z}_{ih}), \\ 0 & \text{otherwise.} \end{cases} \quad (21)$$

Extensive details on model-based clustering and parameter estimation are given by McNicholas (2016a).

3 A Model To Cluster Functional Data

3.1 Model Formulation

From the previous section we saw that the log-likelihood for a GP with the observed output vector \mathbf{y} and corresponding input vector \mathbf{x} was distributed according to a multivariate Gaussian distribution (8). When clustering GPs, the goal will be to find clusters that contain processes which have similar paths. The meaning of similar path refers not only to how close two processes’ values are but also to how similar their shapes are (smooth, wiggly, etc.). Now let us define the notation used for the model: the i th GP will have output vector \mathbf{y}_i , input vector \mathbf{x}_i , and

$$p(\mathbf{y}_i | \boldsymbol{\theta}_i, \mathbf{x}_i) = \exp \left(-\frac{1}{2} \left\{ \mathbf{y}_i \mathbf{K}^{-1} \mathbf{y}_i^\top + \log |\mathbf{K}| + n \log 2\pi \right\} \right). \quad (22)$$

The density in (22) is the probability density function (p_g) used for the finite mixture model shown next:

$$p(\mathbf{y}_i|\boldsymbol{\theta}, \mathbf{x}_i) = \sum_{g=1}^G \pi_g p_g(\mathbf{y}_i|\boldsymbol{\theta}_g, \mathbf{x}_i), \quad (23)$$

where $\boldsymbol{\theta}_g = \{l_g, \sigma_{fg}, \sigma_{ng}\}$ is the set of hyper-parameters for the g th cluster. Because the likelihood of a GP is a Gaussian distribution with covariance matrix \mathbf{K} , the complete-data likelihood is given by

$$\mathcal{L}_c(\boldsymbol{\varphi}) = \prod_{i=1}^n \sum_{g=1}^G [\pi_g \phi(\mathbf{y}_i | \mathbf{0}, \mathbf{K}_g)]^{z_{ig}}, \quad (24)$$

where \mathbf{K}_g is the covariance matrix corresponding to cluster g and ϕ is the Gaussian density function. An SE covariance kernel is used as the prior on the function space, i.e.,

$$k(\mathbf{x}_i, \mathbf{x}_j) = \sigma_f^2 \exp\left(-\frac{1}{2l^2}|\mathbf{x}_i - \mathbf{x}_j|^2\right) + \sigma_n^2 \delta_{ij}. \quad (25)$$

This means that observations are not perfectly interpolated from the GP; instead, they are corrupted by i.i.d. noise σ_n^2 . The goal is to recover the G sets of kernel hyper-parameters $\boldsymbol{\theta}_g = (l_g, \sigma_{fg}^2, \sigma_{ng}^2)$ and the mixing parameters $\boldsymbol{\pi} = (\pi_1, \dots, \pi_G)$, and thence to estimate the latent variables $\mathbf{z}_1, \dots, \mathbf{z}_n$.

3.2 GP Parameter Estimation

The first step is to estimate each GP's kernel hyperparameters. The set of kernel hyper-parameters for the i th GP is denoted by: $\boldsymbol{\Theta}_i = \{l_i, \sigma_{fi}, \sigma_{ni}\}$. In this step, the maximized kernel hyper-parameters for each GP — l_i^{\max} , σ_{fi}^{\max} , and σ_{ni}^{\max} — are estimated. To find these maximized hyper-parameters, an MLE solution is found using gradient ascent, starting with the log-likelihood i.e.,

$$\log p(\mathbf{y}_i|\mathbf{x}, \boldsymbol{\Theta}_i) = -\frac{1}{2} \left\{ \mathbf{y}_i \mathbf{K}^{-1} \mathbf{y}_i^\top + \log |\mathbf{K}| + n \log 2\pi \right\}. \quad (26)$$

The derivative is then taken w.r.t. to the kernel hyper-parameters

$$\frac{\partial}{\partial \boldsymbol{\Theta}_i} \log p(\mathbf{y}|\mathbf{x}, \boldsymbol{\Theta}_i) = \frac{1}{2} \mathbf{y}^\top \mathbf{K}^{-1} \frac{\partial \mathbf{K}}{\partial \boldsymbol{\Theta}_i} \mathbf{K}^{-1} \mathbf{y} - \frac{1}{2} \text{tr} \left(\mathbf{K}^{-1} \frac{\partial \mathbf{K}}{\partial \boldsymbol{\Theta}_i} \right) = \frac{1}{2} \text{tr} \left([\boldsymbol{\alpha} \boldsymbol{\alpha}^\top - \mathbf{K}^{-1}] \frac{\partial \mathbf{K}}{\partial \boldsymbol{\Theta}_i} \right), \quad (27)$$

where $\boldsymbol{\alpha} = \mathbf{K}^{-1}\mathbf{y}$. The partial derivatives for l_i , σ_{fi} , and σ_{ni} are calculated from the first derivatives of the kernel function:

$$\frac{\partial \mathbf{K}}{\partial l_i} = \sigma_{fi}^2 \exp \left\{ -\frac{1}{2l_i^2}(x_i - x_j)^2 \right\} (x_i - x_j)^2 l_i^{-3}, \quad (28)$$

$$\frac{\partial \mathbf{K}}{\partial \sigma_{fi}} = 2\sigma_{fi} \exp \left\{ -\frac{1}{2l_i^2}(x_i - x_j)^2 \right\} (x_i - x_j)^2, \quad (29)$$

$$\frac{\partial \mathbf{K}}{\partial \sigma_{ni}} = \begin{cases} 2\sigma_{ni} & \text{if } x_i = x_j, \\ 0 & \text{otherwise.} \end{cases} \quad (30)$$

After finding the gradient for the likelihood, a gradient ascent algorithm is used to find a sufficiently close solution. This algorithm is given by repeating the following until a convergence criterion is attained:

$$\begin{aligned} l_i^{\text{update}} &:= l_i^{\text{old}} + \lambda \frac{\partial}{\partial l_i} \log p(\mathbf{y}_i | \mathbf{x}, l_i^{\text{old}}) \\ \sigma_{fi}^{\text{update}} &:= \sigma_{fi}^{\text{old}} + \lambda \frac{\partial}{\partial \sigma_{fi}} \log p(\mathbf{y}_i | \mathbf{x}, \sigma_{fi}^{\text{old}}) \\ \sigma_{ni}^{\text{update}} &:= \sigma_{ni}^{\text{old}} + \lambda \frac{\partial}{\partial \sigma_{ni}} \log p(\mathbf{y}_i | \mathbf{x}, \sigma_{ni}^{\text{old}}). \end{aligned} \quad (31)$$

After maximizing the kernel hyper-parameters, we have $\hat{\boldsymbol{\Theta}} = \{\hat{\boldsymbol{\Theta}}_1, \hat{\boldsymbol{\Theta}}_2, \dots, \hat{\boldsymbol{\Theta}}_n\}$, where $\hat{\boldsymbol{\Theta}}_1 = \{l_1^{\text{max}}, \sigma_{f1}^{\text{max}}, \sigma_{n1}^{\text{max}}\}$ denotes the maximized kernel hyper-parameters for the first GP, $\hat{\boldsymbol{\Theta}}_2$ denotes the hyper-parameters for GP 2, and so on.

3.3 Cluster Parameter Estimation

The model seeks to cluster the processes and make inferences on the latent variables. A modified EM approach is used. First, the mixing proportion and cluster hyper-parameters are initialized randomly, i.e., we initialize $\boldsymbol{\pi}$, \mathbf{l} , $\boldsymbol{\sigma}_f$ and $\boldsymbol{\sigma}_n$, where $\mathbf{l} = \{l_1, l_2, \dots, l_G\}$, $\boldsymbol{\sigma}_f = \{\sigma_{f1}, \sigma_{f2}, \dots, \sigma_{fG}\}$, and $\boldsymbol{\sigma}_n = \{\sigma_{n1}, \sigma_{n2}, \dots, \sigma_{nG}\}$. Next, each GP's ($\mathcal{GP}_1, \dots, \mathcal{GP}_n$) responsibilities are calculated for each of the G clusters to get $n \times G$ responsibilities

$$\hat{r}_{ig} = \frac{\pi_g \phi(\mathbf{y}_i | \mathbf{0}, \mathbf{K}_g)}{\sum_{h=1}^G \pi_h \phi(\mathbf{y}_i | \mathbf{0}, \mathbf{K}_h)}, \quad (32)$$

where \hat{r}_{ig} represents the responsibility, or conditional expected value, of the i th process belonging to the g th cluster, $\hat{r}_{ig} \triangleq \hat{z}_{ig}$. After the responsibilities are calculated, the mixing proportions $\boldsymbol{\pi}$ are conditionally maximized on these responsibilities:

$$m_g = \sum_{i=1}^n r_{ig}, \quad \pi_g = \frac{m_g}{m},$$

where $m = \sum_{g=1}^G m_g$, m_g is the responsibility for cluster g and, as usual, π_g is the g th mixing proportion. The kernel hyper-parameters specific for each cluster — l_g , σ_{fg} , and σ_{ng} — are then updated, where l_g is the length-scale parameter for cluster g , σ_{fg} is the height parameter for cluster g , and σ_{ng} is the noise parameter for cluster g :

$$l_g = \frac{1}{m_g} \sum_{i=1}^n \hat{r}_{ig} l_i^{\max}, \quad (33)$$

$$\sigma_{fg} = \frac{1}{m_g} \sum_{i=1}^n \hat{r}_{ig} \sigma_{fi}^{\max}, \quad (34)$$

$$\sigma_{ng} = \frac{1}{m_g} \sum_{i=1}^n \hat{r}_{ig} \sigma_{ni}^{\max}. \quad (35)$$

This is done by weighting the maximized hyper-parameters, σ_{fi}^{\max} , l_i^{\max} , and σ_{ni}^{\max} , by their respective cluster responsibility \hat{r}_{ig} .

This scheme, of calculating the responsibilities then updating the cluster parameters, is repeated until some convergence criterion is met. In this case, when the change in expected complete-data log likelihood at iteration t , defined as the expectation of the complete-data log likelihood: $\mathcal{Q}(\boldsymbol{\varphi}^t, \boldsymbol{\varphi}^{t-1}) = \mathbb{E}[\log(\mathcal{L}_c(\boldsymbol{\varphi}^t)) | \mathbf{y}, \boldsymbol{\varphi}^{t-1}]$ becomes small, i.e., until

$$|\mathcal{Q}(\boldsymbol{\varphi}^t, \boldsymbol{\varphi}^{t-1}) - \mathcal{Q}(\boldsymbol{\varphi}^{t-1}, \boldsymbol{\varphi}^{t-2})| < \epsilon.$$

3.4 Numerical Issues

At each iteration of gradient ascent, the GP's likelihood gradient needs to be computed:

$$\frac{\partial}{\partial \boldsymbol{\Theta}_i} \log p(\mathbf{y}_i | \mathbf{x}, \boldsymbol{\Theta}_i) = \frac{1}{2} \text{tr} \left(\left[\boldsymbol{\alpha} \boldsymbol{\alpha}^\top - \mathbf{K}^{-1} \right] \frac{\partial \mathbf{K}}{\partial \boldsymbol{\Theta}_i} \right). \quad (36)$$

This operation requires inverting a $t \times t$ matrix \mathbf{K}^{-1} . Inverting large matrices are notoriously computationally unstable. This is especially true when matrices are not full rank (or sufficiently close) and eigenvalues become very large or very small. One solution is to first decompose the matrix into lower triangular form: $\mathbf{K} = \mathbf{L} \mathbf{L}^\top$. The lower triangle \mathbf{L} is then inverted: $\mathbf{K}^{-1} = (\mathbf{L}^{-1})^\top \mathbf{L}^{-1}$. We use the R (R Core Team, 2017) package **FastGP** (Gopalan and Bornn, 2016), which implements the package **RcppEigen** (Bates and Eddelbuettel, 2013) to invert the decomposed matrix.

4 Simulation Studies

This section will first look at two cases of simulated data. The hyper-parameters $\boldsymbol{\theta} = \{\mathbf{l}, \boldsymbol{\sigma}_f\}$ and the mixing proportions $\boldsymbol{\pi}$ will vary on the simulated sets. The method developed in the

previous section will then be applied to recover the hyper-parameters and classify each GP into their respective groups. For the two simulation studies, noiseless squared exponential covariance functions will be used. Meaning, a perfectly interpolated, noiseless process is observed for the simulation.

4.1 Simulation I

The first simulation starts with generating 30 GPs. The processes are generated on the interval $[0, 10]$ with $T = 7$ evenly spaced realizations, i.e., each process has seven values spread evenly on the interval. In all, 10 of the 30 GPs are generated from a multivariate normal distribution (using the R package `mvtnorm` (Genz and Bretz, 2009)) where the covariance matrix was constructed using an SE covariance kernel with hyper-parameters $l = 1$ and $\sigma_f = 3$. The remaining 20 were generated similarly but with a covariance matrix constructed with hyper-parameters $l = 3$ and $\sigma_f = 3$.

After running the algorithm described in Section 3, estimates for the set of hyper-parameters and mixing proportion were recorded (Table 1). The mixing proportion is easily identified and accurately estimated. Using the MAP classification, the algorithm was able to correctly classify each process. Table 1 gives the mean parameter estimates and standard errors. This was done by randomly (initializing the parameters from a random uniform draw) starting the algorithm 10 times and calculating the mean and standard error from these 10 starts.

Table 1: Simulation I, mean value for recovered hyper-parameters with standard error. Calculated by randomly restarting the algorithm 10 times.

Parameter	Truth	Mean Estimate	Standard Error
π_1	0.33	0.33	0
π_2	0.67	0.67	0
l_1	1	1.22	0.005
l_2	3	3.08	0.02
σ_{f1}	3	2.09	0.028
σ_{f2}	1	1.32	0.049

Once the processes are coloured by their MAP classification (Figure 1), one can visually see the difference between the two process clusters. The processes ($g = 2$, blue) with the larger length-scale $l = 3$ are smoother compared to those generated from the process with length-scale $l = 1$.

The length-scale parameter l was also readily recovered in this scenario, producing similar estimates to the true hyper-parameter. The hyper-parameter σ_{f1} , which, recall, controls the functions variance (in y), is not near the true parameter value. One reason for this could be because this cluster has a comparatively small length-scale $l = 1$, which models the relative

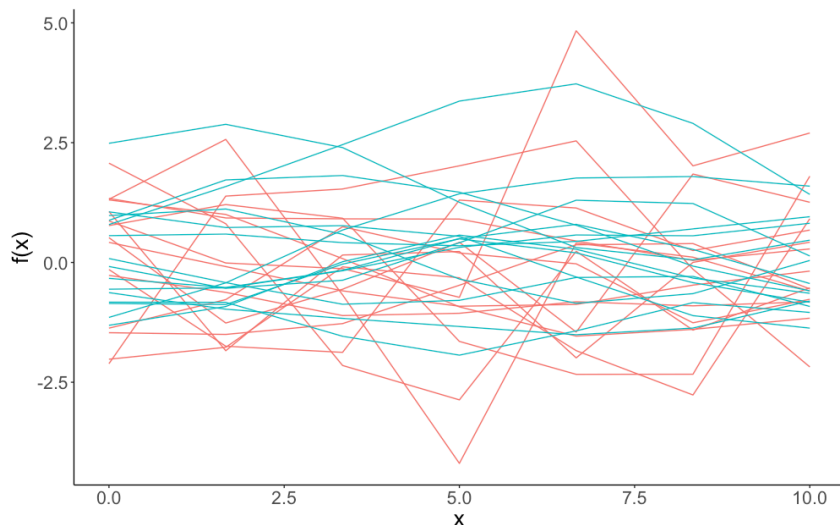


Figure 1: The 30 GPs from Simulation I, coloured by MAP classification. Red lines are cluster $g = 1$ and blue lines are cluster $g = 2$.

correlation between the points. If this is true, preference to model the processes height variation is modelled more precisely with l than with σ_f .

4.2 Simulation II

The second simulation was carried out by first generating 20 GPs. Ten were generated from an SE covariance kernel with hyper-parameters $l = 1$ and $\sigma_f = 1$. The remaining 10 GPs were generated from a covariance kernel with hyper-parameters $l = 2$ and $\sigma_f = 2$. Similarly to Simulation I, the GPs were generated first by constructing the covariance matrix, then by generating random samples using the R package `mvrnorm`. In all, $T = 9$ equally spaced observed values were recorded for each GP (Figure 2). Based on the plot in Figure 2, there seem to be no clear distinction or natural groups of processes. After coloring the processes by their (correct) classifications (Figure 3), there is still ambiguity about the two groups separation.

Again, the method accurately recovers the mixing parameter and length-scale (Table 2). However, for cluster 1, the length-scale l is slightly overestimated and the method inflates σ_f to account for the height variance in y . The parameter estimates were calculated by randomly starting the algorithm 10 times and using the mean estimate. The processes also look very similar between groups, and this solution might seem unconvincing if true group labels were unknown.

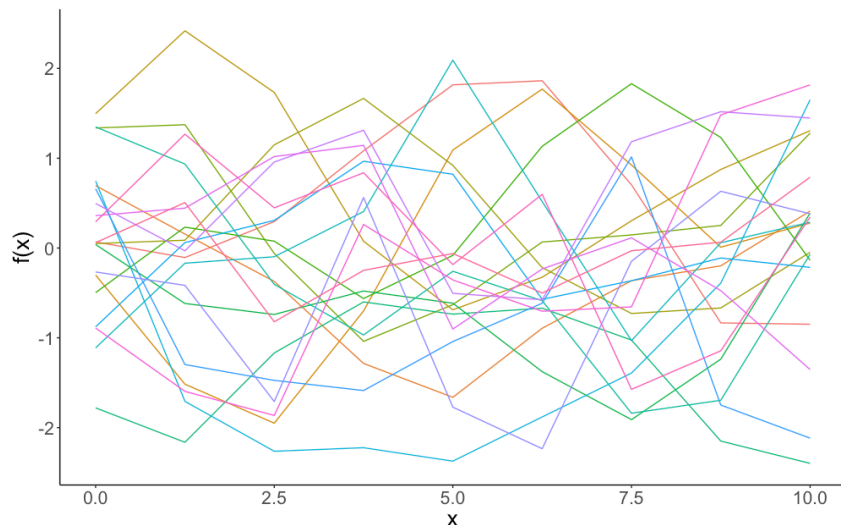


Figure 2: The 20 GPs from Simulation II, generated from two different kernel hyper-parameter settings.

Table 2: Simulation II, mean value for recovered hyper-parameters with standard error. Calculated by randomly restarting the algorithm 10 times.

Parameter	Truth	Mean Estimate	Standard Error
π_1	0.5	0.52	0.002
π_2	0.5	0.48	0.002
l_1	1	1.33	0.016
l_2	2	2.06	0.008
$\sigma_{f\ 1}$	1	1.82	0.034
$\sigma_{f\ 2}$	2	1.84	0.031

5 Costal Rainfall in British Columbia

This section will look at historical monthly precipitation data for the BC coastal region of Tofino. These data are recorded by the Government of Canada and collected from the weather station Tofino A. These data were derived from the following resources available in the public domain: http://climate.weather.gc.ca/climate_data/monthly_data_e.html (Government of Canada, 2007). Total monthly precipitation was recorded from January 1990 to December 2000 (Figure 4). The ten years will be treated as independent GPs. This analyses will use an SE covariance function, with additive measurement noise assumed to be present. Thus, $\theta = \{l, \sigma_f, \sigma_n\}$ will be estimated and modelled. Note that the observed outputs \mathbf{y} will be (artificially) connected by lines for illustrative purposes (Figure 4).

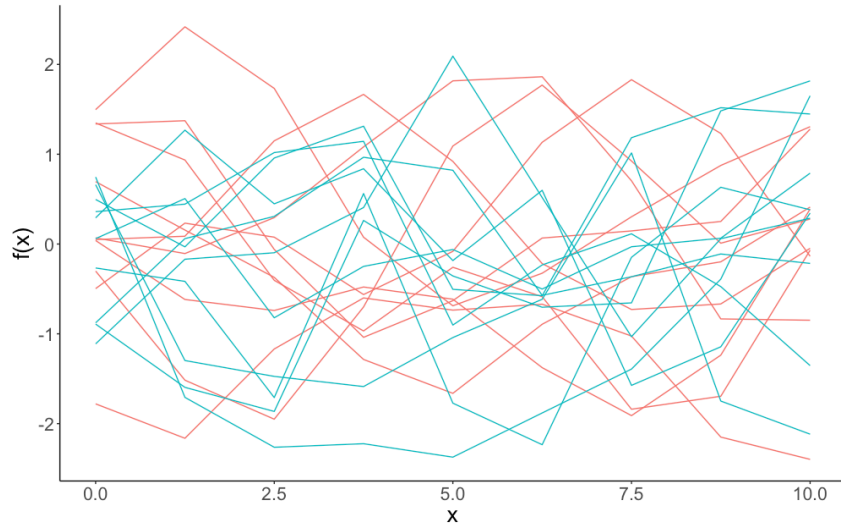


Figure 3: The 20 GPs from Simulation II, classified by their MAP. Red lines are cluster 1, blue lines are cluster 2.

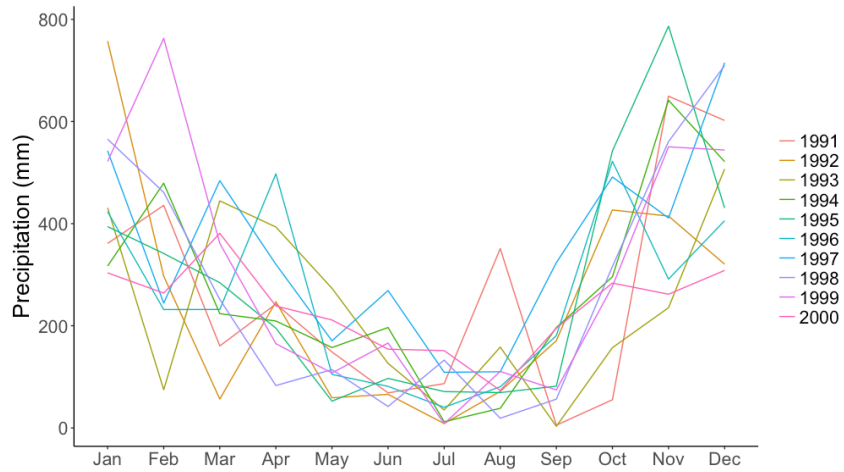


Figure 4: Monthly precipitation for the Tofino coastal region of B.C., Canada. The points are (artificially) connected between months for illustrative purposes, there are 12 measurements per year.

First, the data are centered and scaled such that the mean is 0 and standard deviation is 1. The maximized hyper-parameters are fitted as shown in Figure 5.

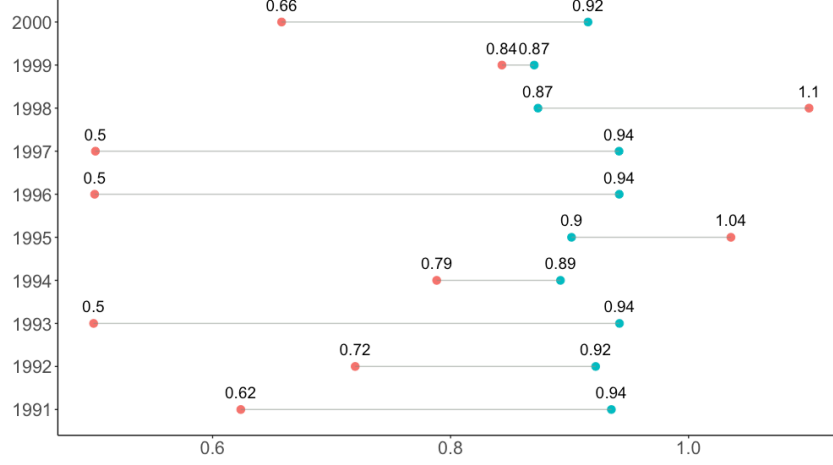


Figure 5: Optimized hyper-parameters for the ten years of precipitation data. Red dots are the l parameter, blue dots are σ_f . The years 1995 and 1998 were classified into a separate cluster, they're the only years in which σ_f is less than l .

There seem to be two groups emerging, six with a smaller length-scale (years 1991, 1992, 1993, 1996, 1997, 2000) and four years with a larger length-scale (years 1994, 1995, 1997, 1998), where a smaller length-scale suggests time points are less correlated relative to time (month). In this case, the years with a smaller length-scale suggest monthly rainfall are less correlated month to month than those with a larger length-scale. After clustering, the ten years are grouped by their MAP classification into two groups (Table 3).

Group two (“irregular”, $\pi_2 = 0.16$) contains the years 1995 and 1998, and the rest are classified into group one (“regular”, $\pi_1 = 0.84$). This is illustrated in Figure 6, where the years are coloured by their MAP classifications.

Cluster 2 contains only years where there was a change from El Niño to La Niña, i.e. the year started with warm enough ocean temperatures to classify it as an El Niño period, and by the end of the year the ocean had cooled enough to be classified as La Niña. The two years (1995, 1998) picked from the classification as belonging to a different cluster correspond to years where rainfall patterns had comparatively larger length-scale parameters. Some years (1992, 1994, and 1999) had comparatively neutral optimized length-scale parameters ($0.72 \leq l \leq 0.84$), which is in between the two cluster’s estimated length-scale parameters but closer to that for Cluster 1, $\mathbf{l} = \{l_1 = 0.7, l_2 = 1.02\}$. The two clusters shared similar height variation (σ_f) and noise (σ_n) parameters as shown in Table 4. The parameter estimates shown represent the mean value and standard error after running the algorithm 10 times, randomly starting the parameters, $\theta = \{\mathbf{l}, \sigma_f, \sigma_n\}$, with different values.

In Figure 7 two years are plotted side by side along with their predictive distribution

Table 3: Year with their MAP classification, related weather events, and their cluster soft classification.

Year	Cluster	Special Event	P(Cluster 1)
1991	1	El Niño	0.99
1992	1	El Niño	0.84
1993	1	None	1
1994	1	El Niño	0.93
1995	2	El Niño to La Niña	0.29
1996	1	La Niña	1
1997	1	El Niño	0.99
1998	2	El Niño to La Niña	0.20
1999	1	La Niña	0.73
2000	1	La Niña	1

Table 4: Clustering results, parameters recovered. These estimates are the mean and standard error calculated by running the algorithm 10 times from random starts. The clusters differed mainly with respect to their length-scale parameter l .

Parameter	Mean Estimate	Standard Error
π_1	0.84	0.011
π_2	0.16	0.011
l_1	0.7	0.002
l_2	1.02	0.008
σ_{f1}	0.93	0.001
σ_{f2}	0.89	0.001
σ_{n1}	0.043	0.001
σ_{n2}	0.055	0.001

\mathbf{f}_* from Equation 13, the estimated function for unobserved values between data points. The blue line (1998, cluster two) is comparatively smoother, the length-scale is larger and changes in output (rainfall) can be accounted for by measurement noise. This is shown as the blue line passes nearby (but not through) some red crosses. Oppositely, the green line (1993, cluster one) is characterized with a smaller length-scale l and smaller noise σ_n . With a smaller l , the function has more flexibility to model the sharp increases/decreases with little noise and, therefore, passes through the points very precisely.

From further consideration of the estimated cluster parameters in Table 4, Cluster 2's years tend towards a larger length-scale compared to cluster one. This suggests years where El Niño changes to La Niña, rainfall patterns change more smoothly (i.e., are more correlated) across months as opposed to regular weather years.

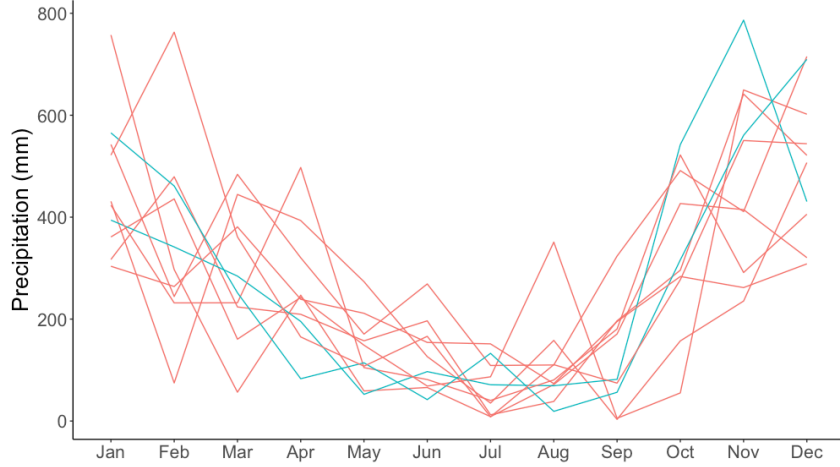


Figure 6: Tofino monthly precipitation coloured by their MAP classification.

6 Discussion

A method for clustering functional data has been introduced to cluster coastal rainfall data from BC. First, the hyper-parameters that make up a GP were optimized through a gradient-based maximum likelihood optimizer. The usual EM algorithm for finite Gaussian mixture models was then modified. Instead of maximizing the standard covariance matrix, hyper-parameters for a kernel function that measures correlation in \mathbf{x} were optimized. The covariance matrix was then constructed from the optimal kernel parameters. Herein, we take G as known; however, future work should consider unknown number of groups using methods such as entropy to select G . It is also noted that missing, or incomplete data can be handled by the model, either by using the predictive distribution to impute the missing data or by ignoring the missing values. This is possible because the model makes inference on the underlying hyper-parameters of the kernel, and not the particular index set of the process.

Two simulation studies were performed. When GPs from different distributions had a large difference in their length-scale parameter l (i.e., 1 versus 3), parameters were readily recovered. When GPs had similar length-scale parameters, l was recovered but σ_f tended to shrink towards a common estimate between both clusters. The application to the rainfall data from the coastal region of Tofino, B.C discovered two groups of years, one which contained “regular” years and the other “irregular” years. The irregular years consisted only of years that had both El Niño and La Niña events. These results suggest El Niño events can be classified based on their kernel hyper-parameters. The data were standardized to have a zero mean function, implying correlation between rainfall patterns month-to-month can

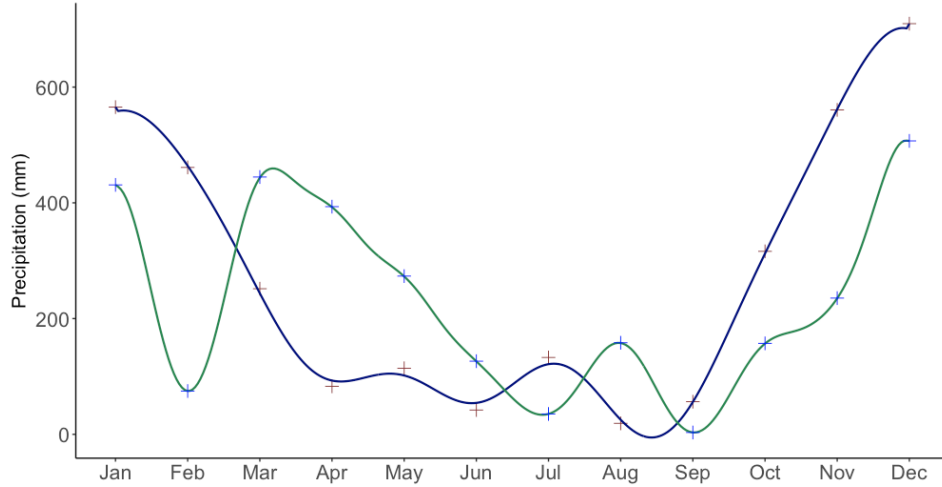


Figure 7: Two years of data plotted alongside their predictive distribution. The blue line (year 1998) is smoother than the green line (year 1993). Mainly because its characterized by a higher noise parameter (σ_n^2), which is able to account for change in height as measurement noise independent of the underlying function. Whereas the green line must move quicker (through a smaller length-scale) to fit the points.

discriminate El Niño events (as apposed to magnitude of rainfall).

References

- Bates, D. and D. Eddelbuettel (2013). Fast and elegant numerical linear algebra using the RcppEigen package. *Journal of Statistical Software* 52(5), 1–24.
- Bin, S. and Y. Wenlai (2013). Application of gaussian process regression to prediction of thermal comfort index. In *2013 IEEE 11th International Conference on Electronic Measurement Instruments*, Volume 2, pp. 958–961.
- Dempster, A. P., N. M. Laird, and D. B. Rubin (1977). Maximum likelihood from incomplete data via the EM algorithm. *Journal of the Royal Statistical Society: Series B* 39, 1–38.
- Genz, A. and F. Bretz (2009). *Computation of Multivariate Normal and t Probabilities*. Lecture Notes in Statistics. Heidelberg: Springer-Verlag.

- Gopalan, G. and L. Bornn (2016). *FastGP: Efficiently Using Gaussian Processes with Rcpp and RcppEigen*. R package version 1.2.
- Government of Canada (2007). Monthly Precipitation Data, Tofino A. http://climate.weather.gc.ca/climate_data/monthly_data_e.html. Accessed 2018-08-05.
- Gudmundson, C. and A. M. Babkina (2003). *El Niño Overview and Bibliography*. Hauppauge, New York: Nova Science Publishers, Inc.
- McNicholas, P. D. (2016a). *Mixture Model-Based Classification*. Boca Raton: Chapman & Hall/CRC Press.
- McNicholas, P. D. (2016b). Model-based clustering. *Journal of Classification* 33(3), 331–373.
- R Core Team (2017). *R: A Language and Environment for Statistical Computing*. Vienna, Austria: R Foundation for Statistical Computing. ISBN 3-900051-07-0.
- Rasmussen, C. E. (2005). *Gaussian Processes for Machine Learning*. Cambridge: MIT Press.
- Ward, P. J., B. Jongman, M. Kumm, M. D. Dettinger, F. C. Spera Weiland, and H. C. Winsemius (2014). Strong influence of el nino southern oscillation on flood risk around the world. *Proceedings of the National Academy of Sciences* 111(44), 15659–15664.